IEEE Transactions on Power Systems, vol. 10, no. 1, February 1995, pp. 512–522.

On Bifurcations, Voltage Collapse and Load Modeling

Claudio A. Cañizares, Member
University of Waterloo
Elec. & Comp. Eng. Dep.
Waterloo, ON, Canada N2L 3G1

Abstract—This paper discusses the relation between bifurcations and power systems stability through a thorough analysis of several examples, to clarify some ideas regarding the usefulness and limitations of bifurcation theory in network studies and operation, particularly in voltage stability related issues. Different types of load models are used in a sample system to analyze their effect on system stability and bifurcation. Finally, the Ecuadorian National Interconnected System (SNI in Spanish) is used to depict and discuss the effect of load modeling in saddle-node bifurcation analysis of real power systems.

Keywords: bifurcations, voltage collapse, load modeling, stability, eigenvalue analysis.

I. INTRODUCTION

During the past decade utilities have reported serious complications in maintaining network stability in their power systems, particularly voltage stability, as some events occur and parameters change in the system [1]–[3]. The study of several cases has led the power systems community to identify different causes for this problem.

Hopf and saddle-node bifurcations have been recognized as some of the reasons, albeit not the only ones, for voltage stability problems in a variety of power system models [4]–[9]. Local bifurcations are detected by monitoring the eigenvalues of the current operating point. As certain parameters in the system change slowly, allowing the system to quickly recover and maintain a stable operating point, the system eventually turns unstable, either due to one of the eigenvalues becoming zero (saddle-node, transcritical, pitchfork bifurcations), or due to a pair of complex conjugate eigenvalues crossing the imaginary axes of the complex plane (Hopf bifurcation). The instability of the system is reflected on the state variables, usually represented by frequency, angles and voltages, by an oscillatory behavior or a continuos change (voltage decrease, i.e., collapse, *and* frequency and angle increase, i.e., loss of synchronism). In some cases these bifurcations can be associated to the power transfer limit of the transmission system; in other instances the bifurcations appear due to voltage control problems, like fast acting automatic voltage regulators (AVR) in the generator [10], or voltage dependent current order limiters (VDCOL) in HVDC links [7]. In all cases these bifurcations occur on very stressed systems, i.e., the region of stability for the current operating point (stable equilibrium point or s.e.p.) is small, hence, the system is not able to withstand small perturbations and becomes unstable. Although there are reports of these bifurcations occurring in unstressed systems [11], this cannot be considered typical, since power system controls are designed so that eigenvalues of several operating points are well into the left half complex plane.

Some voltage collapse problems can also be associated to voltage control devices like under-load tap changer (ULTC) transformers or AVRs [12]–[15]. In some of these cases, but not all, the voltage controls force the eigenvalues to instantaneously jump into the unstable region, making the system immediately unstable. This phenomena is not directly associated to a bifurcation, since the eigenvalues do not go through zero or the imaginary axis. Nevertheless, transcritical bifurcation theory can be used to explain the phenomena when AVR limits are assumed to apply gradually [13].

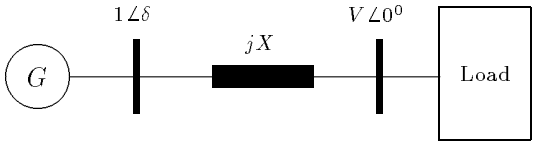

Fig. 1. Sample system for bifurcation analysis.

Recent literature shows that there is not a consensus in the power system community regarding the importance and usefulness of bifurcation analysis of power systems (e.g., [16]). Therefore, this paper concentrates mainly on clarifying some issues regarding local saddle-node bifurcations, by clearly depicting their effect and relationship to the voltage collapse phenomena for different load models in several sample systems. This does not rule out the fact that other type of bifurcations, i.e., transcritical or Hopf, do also occur in real systems, with similar catastrophic results for system (voltage) stability. Although bifurcations cannot be considered as the only cause for voltage stability problems, as discussed above, the effect of saddle-node bifurcations in system stability cannot be overlooked based on this sole argument.

The final section of this paper concentrates on applying the results obtained for the sample systems to the 115 bus SNI Ecuadorian system [17], to discuss some of the applications and shortcomings of bifurcation theory in a more realistic environment.

II. EXAMPLES

In this section the stability of four sample systems is thoroughly analyzed. Local saddle-node bifurcations are depicted and discussed to highlight some of their main characteristics. All four cases discussed here are based on the system depicted in Fig. 1.

The generator is modeled with the classical second order mechanical differential equations. The damping torques are assumed to have a relatively large value to indirectly simulate the effect of damper windings in the generator. The AVR is modeled by keeping the generator terminal voltage constant at 1 pu, but no limits are included in this simple model. Although this is not a detailed model of the generator by any means, it gives a good starting point for analyzing the significance of saddle-node bifurcations in system stability, without adding unnecessary complexities that only obscure some of the questions that are being addressed in this paper. For an analysis of bifurcations in detailed generator models review reference [11].

The transmission system is simply modeled as a constant lumped reactance, which is a typical representation of these elements in transient stability studies, where the system frequency oscillates slowly around the nominal value (e.g., 60Hz), allowing for a quasi-steady state or phasor analysis of the system. Consequently, this type of methodology cannot be used to simulated high frequency voltage problems in the system.

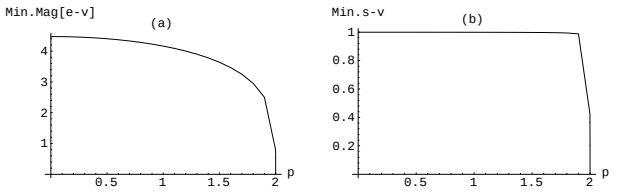

Fig. 2. (a) Minimum magnitude of the s.e.p. (u.e.p.) eigenvalues, and (b) minimum singular value of the s.e.p. as a function of P. Notice the sharp change in the eigenvalues magnitude and singular values when the system approaches bifurcation.

The four study cases are obtained by changing the load model at the receiving end of the transmission line, as shown below. Some of these examples are discussed from a different point of view in [18].

A. *Generator-Infinite Bus*

The first load model is an infinite bus, which is drawing active power $P > 0$ from the generator at a constant voltage $V > 0$. This is the classical generator-infinite bus model utilized to introduce basic ideas of angle and frequency stability in power systems, hence, the same example is used here to introduce some basic concepts of bifurcation analysis. For this simple case, differential equations (1) represent the system.

$$\begin{aligned} \dot{\delta} &= \omega \\ \dot{\omega} &= \frac{1}{M}\left[P - \frac{V}{X}\sin(\delta) - D\omega\right] \end{aligned} \tag{1}$$

All equilibrium points can be easily found by solving equations (1) with $[\dot{\delta}\ \dot{\omega}]^T = \mathbf{0}$, yielding equilibria $(\delta_0, 0)$, and $(\pm\pi - \delta_0, 0)$ with $\delta_0 = \sin^{-1}(PX/V)$ (other equilibrium points are not of interest). Hence, all the eigenvalues and eigenvectors associated to these equilibria can be calculated from the Jacobian matrix (2).

$$J = D_{(\delta,\omega)} \left[\begin{array}{c} \dot{\delta} \\ \dot{\omega} \end{array}\right]\Bigg|_{(\delta_0,0)} = \left[\begin{array}{cc} 0 & 1 \\ -\frac{V}{MX}\cos(\delta_0) & -\frac{D}{M} \end{array}\right] \tag{2}$$

From the eigenvalues of J it can be readily shown that $(\delta_0, 0)$ is a s.e.p., i.e., all eigenvalues are in the left half complex plane, whereas $(\pm\pi - \delta_0, 0)$ are unstable equilibrium points (u.e.p.) of type one, i.e., only one eigenvalue is on the right half plane. If P changes, i.e., the system load changes, then for any value of $P > P_{max} = V/X$, one eigenvalue of J becomes zero (J is singular) and no equilibria exist. When $P = P_{max}$, the maximum power transfer point for the transmission system, J is also singular and two equilibrium points $(\pi/2, 0)$ and $(-3\pi/2, 0)$ exist, i.e., the s.e.p. and one u.e.p. have merged. The point $(\pi/2, 0, P_{max})$ corresponds to a saddle-node bifurcation, since it meets all the transversality conditions required for this type of bifurcation in state-parameter space [7, 19, 20].

Figures 2, 3, and 4 were obtained from equations (1) by setting $M = D = 0.1$pu, $X = k = 0.5$pu, and $V = 1$pu. In Fig. 2 the minimum magnitude of the complex eigenvalues and the minimum singular value of the s.e.p. $(\delta_0, 0)$ are plotted for a continuously increasing P load; the u.e.p. $(\pi - \delta_0, 0)$ presents the same profiles. At the value $P_{max} = 2$pu one eigenvalue (singular value) of the s.e.p. and the u.e.p. becomes zero. Observe that the profile of these two measures is highly nonlinear and varies only slightly up to the load level of $P \approx 1.8$, decreasing rapidly after that. Similar profiles can be observed in larger and more detailed modeled systems [4, 9, 21], making these measures inadequate to monitor system proximity to bifurcation.

Other techniques have been proposed to avoid using eigenvalues or singular values for measuring proximity to bifurcation (see reference [22] for a summary). In particular, Transient Energy Function (TEF) techniques have been shown to have a "linear" profile and yield additional information regarding the stability of the system [23], making these methods more suited for measuring proximity to bifurcation but at a higher computational cost. For the sample

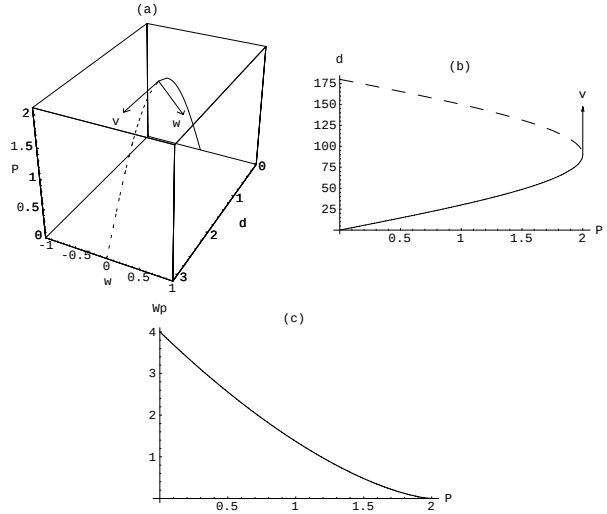

Fig. 3. Bifurcation diagrams: (a) in (δ,ω,P) axes; (b) P-δ node curve; (c) potential energy W_p between s.e.p. and closest u.e.p. Right **v** and left **w** eigenvectors at the bifurcation point are also depicted; note that **v** is tangent to the bifurcation diagram.

system under discussion, the energy can be defined as a summation of the kinetic and the potential energy as shown in (3). The potential energy can be approximated in this case by the integral of the power-angle product, when assuming only small variations of the system frequency (a typical conjecture in transient stability studies).

$$\begin{aligned} V(\delta,\omega,P) &= W_k(\omega) + W_p(\delta,P) \\ &= \frac{1}{2}M\omega^2 + \int_{\delta_0}^{\delta} \Delta T(u,P)\mathrm{d}u \\ &\approx \frac{1}{2}M\omega^2 + \int_{\delta_0}^{\delta}\left[\frac{V}{X}\sin(u) - P\right]\mathrm{d}u \\ &= \frac{1}{2}M\omega^2 + P(\delta_0 - \delta) + \frac{V}{X}\left[\cos(\delta_0) - \cos(\delta)\right] \end{aligned} \tag{3}$$

By using the potential energy distance $V(\delta_u, 0, P)$ between the s.e.p. and the "closest" u.e.p., as depicted in Fig. 3(c), one can get a good idea of the distance to bifurcation, due to the quasi-linear profile of this measure, and also visualize the relative size of the stability region, including all system nonlinearities. The latter property is rather important, since no technique based on eigenvalues or linearizations of the system around equilibrium points can give the user this information, due to the elimination of the nonlinearities that characterize the stability of the system for large perturbations like line openings at fixed load levels. It is interesting to observe that this particular energy function $V(\cdot)$ is the integral of the area of the bifurcation diagrams depicted in Figs. 3(a) and (b), for a chosen load level P (i.e., equal area criterion), being this the reason for the "linear" profile of the TEF; this property has been demonstrated for other system models and energy functions in reference [24]. Similar TEF profiles have also been observed for highly nonlinear AC/DC system models when close to bifurcation [25]. Hence, the energy measurement clearly depict the reduction of the stability region as the system approaches bifurcation, making it more sensitive to small perturbations that can easily drive it to instability.

The continuos lines in Figs. 3(a) and (b) represent the s.e.p.s, and the dashed lines the corresponding "closest" u.e.p.s for each value of the parameter P. Figure 3(b) is the projection of Fig. 3(a) in the (δ, P) plane, yielding a typical "nose" curve for angle variables and a different view of the classical P–δ stability curve. Some interesting observations can be made in these figures:

- The normalized left eigenvector **v** at the bifurcation point is tangent to the bifurcation diagram [26]; hence, by looking

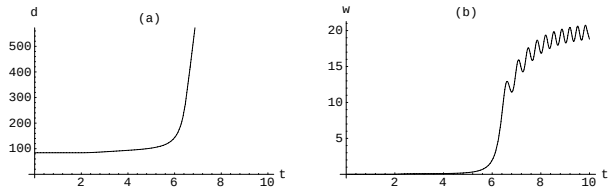

Fig. 4. Time domain simulation for a change in P from 1.99 to 2.01 at $t = 2$s. Observe the slow initial change in the state variables (δ,ω).

at the maximum entries in this vector, one can pinpoint the areas (state variables) that are changing the most and driving the system to bifurcation, so that corrective measures can be taken to avoid stability problems [9, 27]. This eigenvector also yields information regarding the initial dynamics of the system at the bifurcation point [6].

- The normalized right eigenvector **w** at the bifurcation does not have a direct geometric interpretation in bifurcation diagrams, but it has been shown to yield information regarding the equations that are most sensitive to changes at the bifurcation point [9, 27], and can be used to devise a technique to move away from this instability [28]. This eigenvector depends on the time constants (M in the sample system) of the differential equations [26], whereas **v** is independent of them.
- The bifurcation diagram can be used to determine the distance to the bifurcation point, so that an operator knows in state and parameter space how close the system is to the instability point. Nevertheless, this diagram by itself does not yield the size of the stability region associated to the different s.e.p.s depicted in it, and cannot give the operator a sense of the type of perturbations that the system can withstand at some specific load level, unless it is used in conjunction with and "energy" measure that takes into consideration the nonlinearities in the system.

Finally, Fig. 4 depicts the dynamics of the system as the load is increased slightly beyond the bifurcation value; a rather small system perturbation. Notice the separation or lost of synchronism of the generator with respect to the infinite bus, with initial slow dynamics of the state variables (δ, ω) [6]. This particular example does not present any stability problems that could be characterized as voltage collapse, however, it clearly depicts an instability due to a bifurcation problem, and if voltages were allowed to change the angular-frequency instability would necessarily force the voltages to collapse. This is the reason why bifurcation studies should be done considering all system dynamics and not only voltage controls, to correctly capture all the bifurcation phenomena.

B. PQ Dynamic Load

The infinite bus load model is now replaced by a more "realistic" constant active and reactive power model. This model is meant to simulate the behavior of typical static loads when ULTCs are taken into consideration [12]. Furthermore, introducing a dynamic voltage term in the reactive power load roughly simulates the response of induction motors to sudden voltage changes under normal voltage operating conditions [29, 30]. This cannot be considered an accurate model of the actual system load, but allows to introduce and depict some of the stability problems, particularly voltage collapse, that occur when a saddle-node bifurcation is encountered by the system.

The differential equations used to model this sample system are equations (1) plus equation (4) below, and the Jacobian corresponding to an equilibrium point $(\delta_0, 0, V_0, P)$ of this set of equations is represented by (5).

$$\dot{V} = \frac{1}{\tau}\left[-kP - \frac{V^2}{X} + \frac{V}{X}\cos(\delta)\right] \tag{4}$$

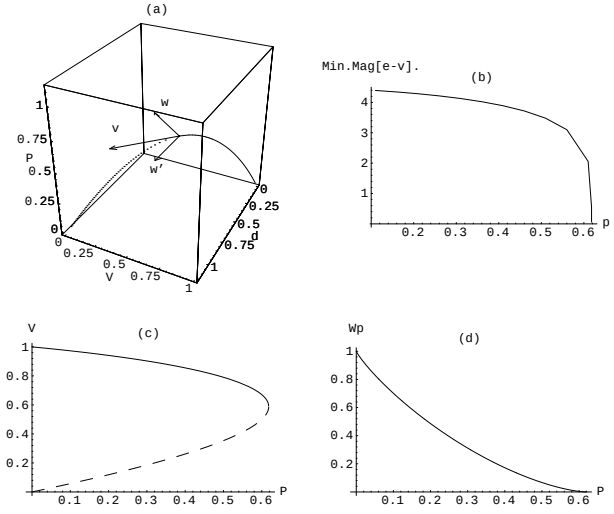

Fig. 5. Bifurcation diagrams: (a) in (δ,V,P) axes; (b) minimum magnitude of s.e.p. eigenvalues as a function of load level P; (b) P-V node curve; (c) potential energy W_p between s.e.p. and closest u.e.p. Right **v** and left **w** eigenvectors at the bifurcation point are depicted. The vector $\mathbf{w}'$ is the projection of **w** onto the (δ,V) plane.

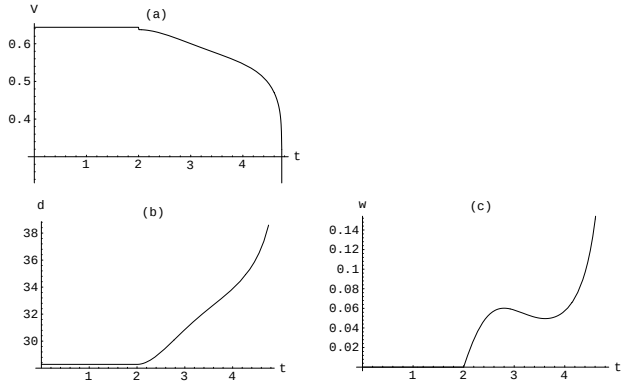

Fig. 6. Time domain simulation for a change in P from 0.61 to 0.62 at $t = 2$s. Observe the fast voltage collapse and the mechanical instability reflected in δ and ω.

$$J = \begin{bmatrix} 0 & 1 & 0 \\ -V/MX\cos(\delta_0) & -D/M & -1/MX\sin(\delta_0) \\ -V/\tau X\sin(\delta_0) & 0 & -1/\tau X[2V - \sin(\delta_0)] \end{bmatrix} \tag{5}$$

Here k is a scalar representing constant power factor, and τ is the time constant of the dynamic voltage term. When $\tau \to 0$, equation (4) becomes an algebraic constraint, however, the dynamics of the system lose physical meaning since this set of differential equations and algebraic constraints cannot be qualified as a "causal" system according Kwatny's et al definition [5]. Furthermore, this system presents a degenerate bifurcation point in state-parameter space where two stable equilibrium points coalesce. For a detailed analysis of these types of system models review references [31]–[33].

Figures 5 and 6 were obtained using the same constant values as in the previous example, and setting $\tau = 1$ms to simulate fast load dynamics in the context of a typical transient stability study. Figure 5(a) depicts a saddle-node bifurcation diagram for δ and V ($\omega = 0$ for all equilibria), i.e., a s.e.p. and a u.e.p. coalesce at a singular point (Fig. 5(b)) for the parameter value $P_{max} = 0.618034$, with equilibria disappearing for values of $P > P_{max}$. P_{max} corresponds again to the point of maximum power transfer, as it is shown in the next section with an R-L load. Figure 5(c) depicts the classical

P-V nose curve, which is a projection of the bifurcation diagram in the (P,V) plane. A similar result as the one depicted in Fig. 3(b), i.e., a P-δ nose curve, can also be obtained here by projecting the bifurcation diagram in the (P,δ) plane; however, in this case the bifurcation occurs at a value of $\delta \approx 30° << 90°$. Observe that the right eigenvector $\mathbf{v}$ is also tangent to the bifurcation diagram at the saddle-node bifurcation point, with the entries in this vector pointing to a voltage problem regardless of the value of $\tau > 0$.

The energy function for this particular system is represented by equation (6) [34]. The results of evaluating the energy difference between the s.e.p.s and corresponding u.e.p.s in the bifurcation diagram of Fig. 5(a) are depicted in Fig. 5(d). Notice once more the quasi-linear profile of the TEF, representing the reduction of the stability region as the system approaches bifurcation.

$$V(\delta,\omega,V,P) = \frac{1}{2}M\omega^2 + P(\delta_0-\delta) + \frac{V}{X}[\cos(\delta_0)-\cos(\delta)] + \frac{1}{2X}(V_0^2-V^2) - kP[\ln(V_0)-\ln(V)] \quad (6)$$

Figures 6 depict the time domain simulation of the differential equations (1) and (4) for a slight increase in load power P. In this plots the same patterns of the previous example appear, i.e., the state variables start changing slowly to then rapidly render the system unstable. In this case, due to the small voltage time constant as compared to the machine inertia, the voltage collapses at $t \approx 5$s rather quickly when compared to the angle and frequency. This particular voltage behavior due to the differences in time constants, have led many researchers to only consider voltage dynamics for the analysis of bifurcations problems, ignoring frequency dynamics. However, the previous example clearly shows that this assumption is not completely justifiable.

This sample system is a classical benchmark for voltage stability studies, due to the characteristic voltage behavior discussed in this section.

C. RL Loads

Now the PQ dynamic load is replaced by an RL dynamic load, i.e., the load is represented by a constant power factor impedance, with the same dynamic voltage term as in the previous case. Hence, differential equations (7) are used to model this particular system, with G representing the load conductance and the slow varying parameter in this example.

$$\begin{aligned} \dot{\delta} &= \omega \\ \dot{\omega} &= \frac{1}{M}\left[V^2G - \frac{V}{X}\sin(\delta) - D\omega\right] \\ \dot{V} &= \frac{1}{\tau}\left[-kV^2G - \frac{V^2}{X} + \frac{V}{X}\cos(\delta)\right] \end{aligned} \quad (7)$$

Using the same constant values as in the previous examples, one obtains Figs. 7 and 8. Figure 7(a) depicts the bifurcation diagram for changes in the parameter G; observe that no bifurcations occur in this case, as shown by the eigenvalues plot of the system equilibria in Fig. 7(b). Furthermore, only one s.e.p. can be obtained for each value of $G \geq 0$. Nevertheless, due to the relation between conductance G and the active power P depicted in Fig. 7(d), this system presents exactly the same P-V nose curve as in the case of the PQ load model (Fig. 7(c)), with all equilibria in this curve being stable. The tip of this nose curve is *not* a bifurcation point, although it corresponds to the system's maximum power transfer point P_{max}, i.e., $|G(1+jk)| = 1/X$ ($G = 4/\sqrt{5} = 1.78885$, and $P_{max} = 0.618034$). The nose curve in this case cannot be considered a bifurcation diagram, since G is the parameter that changes in the system and not P.

Figures 8 corroborate the previous discussion. A relatively large change in G, which takes the system around the maximum power transfer point P_{max}, does not render the system unstable, taking it to a new s.e.p. in spite of the large perturbation.

An exact energy function cannot be found for this sample system, due to the presence of a resistive term in the model [35]. Although an approximate TEF could be constructed in this case, it cannot be readily used as in previous examples to obtain a relative measure of the stability region as the conductance G changes.

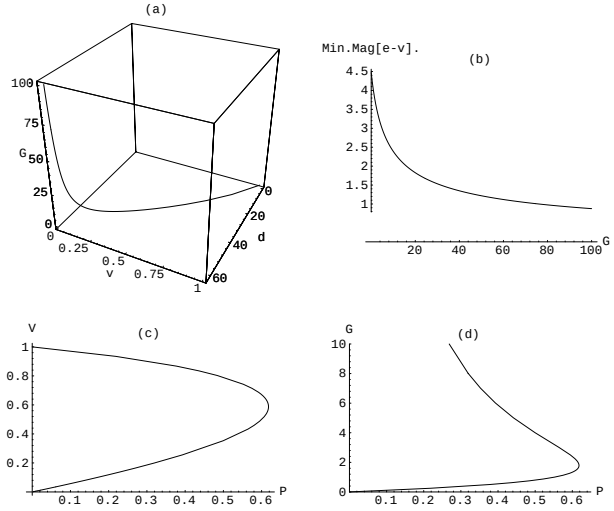

Fig. 7. Bifurcation diagrams: (a) in (δ,V,G) axes; (b) minimum magnitude of s.e.p. eigenvalues as a function of the parameter G; (c) P-V nose curve; (d) P-G curve. Notice that all equilibrium points are stable for any value of the parameter G, even though the P-V nose curve is exactly the same as in the case with the PQ load model.

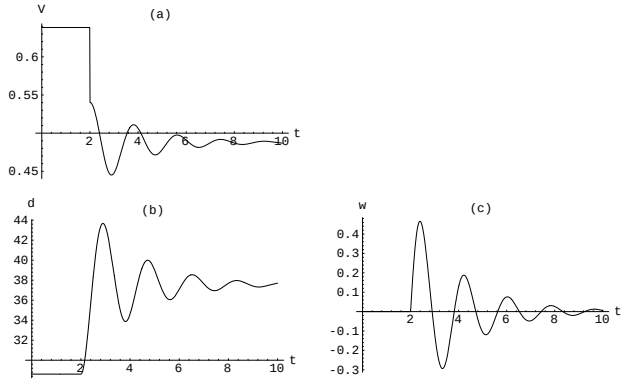

Fig. 8. Time domain simulation for a change in G from 1.5 to 2.5 at $t = 2$s, taking the systems around the maximum power transfer point $P_{max} = 0.618034$pu. Observe that all state variables (δ,ω,V) remain stable.

Finally, the system load is changed to a static RL load model, eliminating the dynamic voltage dependence in equations (7) by setting $\tau = 0$, i.e., the third differential equation becomes an algebraic constraint. Despite this change in load model, and contrary to what happens in the case of the PQ load model when $\tau \to 0$, the results remain *exactly* the same with the only difference that V is allowed to change instantaneously.

III. APPLICATIONS

The foregoing discussion can be directly extended to larger and more complex power system models. Transient stability analysis is typically done on a balanced phasor model of the network, which can be represented by the set of nonlinear differential and algebraic constraints (8), where $\mathbf{x} \in \Re^n$ stands for the state variables, $\mathbf{y} \in \Re^m$ portrays a set of implicitly defined variables, and $\lambda \in \Re$ is a parameter used to simulate slow changing conditions (small

perturbations) in the system.

$$\begin{aligned} \dot{\mathbf{x}} &= \mathbf{f}(\mathbf{x}, \mathbf{y}, \lambda) \\ \mathbf{0} &= \mathbf{g}(\mathbf{x}, \mathbf{y}, \lambda) \end{aligned} \tag{8}$$

This model has the difficulty of not fully representing real physical quantities, which is reflected in the presence of the algebraic constraints $\mathbf{g}(\cdot)$ and the use of reactive powers throughout the equations. Nevertheless, this set of equations can be used to represent any degree of complexity in modeling and system size, within the bounds of the assumptions used to build the model.

For equations (8), the algebraic constraints must meet certain conditions in order for the model to approximate physical reality [5, 7, 26, 31, 32]. Particularly, at equilibrium points $(\mathbf{x}_0, \mathbf{y}_0, \lambda)$, such that $\mathbf{f}(\mathbf{x}_0, \mathbf{y}_0, \lambda) = \mathbf{0}$ and $\mathbf{g}(\mathbf{x}_0, \mathbf{y}_0, \lambda) = \mathbf{0}$, the Jacobian of these constraints $D_y \mathbf{g}|_{(x_0, y_0, \lambda)}$ should be invertible, rendering the system "causal" [5], otherwise singular perturbations or noise techniques must be used to analyze the dynamics of the system [31, 32]. Furthermore, if $D_y \mathbf{g}(\cdot)$ is invertible (nonsingular) along system trajectories, the system can be represented by the set of differential equations

$$\dot{\mathbf{x}} = \mathbf{f}(\mathbf{x}, \mathbf{y}^{-1}(\mathbf{x}, \lambda), \lambda) = \mathbf{F}(\mathbf{x}, \lambda) \tag{9}$$

This reduction is actually unnecessary, since one only needs to check for and remove singularities in the algebraic equations Jacobian. For a detailed discussion on this issues and their relation to bifurcation analysis in power systems review [7, 26].

For bifurcation analysis of this system model, the eigenvalues and eigenvectors of the system Jacobian (10) must be monitored.

$$J = \begin{bmatrix} D_x \mathbf{f}|_0 & D_y \mathbf{f}|_0 \\ D_x \mathbf{g}|_0 & D_y \mathbf{g}|_0 \end{bmatrix} \tag{10}$$

For saddle-node bifurcations in particular, one needs only to look for a singularity of this Jacobian and test for the corresponding transversality conditions [7, 26]. The latter is usually unnecessary since saddle-node bifurcations occur generically in differential equations (9) [19]; nevertheless, under certain operating conditions like remote voltage control, which give the system equations a special symmetry, transcritical bifurcations can also be encountered.

Embedded in this set of equations are the algebraic and/or differential equations representing the load. For this paper a mixed load model represented by equations (11) is used, since it has been shown to adequately represent a variety of system loads in typical transient stability studies [29, 30, 37].

$$\begin{aligned} P_l = &-(P_{l_0} + \Delta P_{l_0}\lambda) - (P_{l_1} + \Delta P_{l_1}\lambda)\left(V_l/V_l^0\right)^2 \\ &-(P_{l_2} + \Delta P_{l_2}\lambda)\left(V_l/V_l^0\right) - \tau_{l_{f_P}}(\dot{\delta}_l - \omega_{n_G}) - \tau_{l_{v_P}}\dot{V}_l \\ Q_l = &-(Q_{l_0} + \Delta Q_{l_0}\lambda) - (Q_{l_1} + \Delta Q_{l_1}\lambda)\left(V_l/V_l^0\right)^2 \\ &-(Q_{l_2} + \Delta Q_{l_2}\lambda)\left(V_l/V_l^0\right) - \tau_{l_{f_Q}}(\dot{\delta}_l - \omega_{n_G}) - \tau_{l_{v_Q}}\dot{V}_l \end{aligned} \tag{11}$$

Here P_l and Q_l are the powers injected by the load, and $V_l \angle \delta_l$ is the load phasor voltage at bus l. P_{l_0}, P_{l_1}, P_{l_2}, Q_{l_0}, Q_{l_1}, and Q_{l_2} are constant weighting factors that define the steady state base load. $\tau_{l_{f_P}}$, $\tau_{l_{v_P}}$, $\tau_{l_{f_Q}}$, and $\tau_{l_{v_Q}}$ represent the time constants of the frequency and voltage dependent dynamic terms, and ω_{n_G} is the system reference frequency; note that these time constants can be set to zero to represent static load models. ΔP_{l_0}, ΔP_{l_1}, ΔP_{l_2}, ΔQ_{l_0}, ΔQ_{l_1}, and ΔQ_{l_2} are used to model a direction of load change as the parameter λ slowly varies. For most bifurcation studies it is assumed that the pattern of load change can be represented with one degree of freedom (λ), and that this evolution of load drives the system to bifurcation. Notice that differential equations (11) can be rewritten as

$$\begin{bmatrix} \dot{\delta}_l - \omega_{n_G} \\ \dot{V}_l \end{bmatrix} = \begin{bmatrix} \tau_{l_{f_P}} & \tau_{l_{v_P}} \\ \tau_{l_{f_Q}} & \tau_{l_{v_Q}} \end{bmatrix}^{-1} \begin{bmatrix} \delta P_l(\delta, \mathbf{V}, \lambda) \\ \delta Q_l(\delta, \mathbf{V}, \lambda) \end{bmatrix}$$

where $\delta P_l(\delta, \mathbf{V}, \lambda)$ and $\delta Q_l(\delta, \mathbf{V}, \lambda)$ are the active and reactive power mismatches at the load buses, respectively.

Although the issue of whether this load model is a "realistic" representation of the actual system load does not pertain to this particular paper, it is a very valid question, since as demonstrated in this paper and others before (e.g., [36]), the results of stability studies are closely related to system modeling, particularly load modeling [37]. This is an old discussion that has not been resolved to the total satisfaction of all the power system community. Nevertheless, the load model must be valid in the context of the tools that are used for stability studies; for instance, very fast dynamics like thyristor switching of motor drives cannot be fully represented in typical transient stability programs, since these tools have been designed to deal with quasi-steady state models, i.e., balanced phasor models that treat transformers and transmission lines as lumped one-phase impedances without any frequency dependence. For fast load dynamics a very detailed model of the whole system is needed, being tools like the EMTP more appropriate environments for analyzing stability of these models; however, these types of studies are very expensive, with costs growing exponentially with system size. Hence, a compromise and a critical view of the results yielded by some of these programs is needed, and bifurcation analysis is not an exception, i.e., the output and cost of these studies are closely related to the models used.

The SNI Ecuadorian system is used in this paper due to its particular voltage stability problems, and also to depict the effect of different load models in saddle-node bifurcation analysis of real systems. The results shown here have been used to confirm suspicions regarding the possible causes of the voltage problems in the system, and to study some possible solutions. The generators in this case are simply model using the second order differential equations with constant terminal voltage used in the previous examples, which is an acceptable model to address the main issues in the present discussion. A continuation method was used to obtain the bifurcation diagrams in Figs. 9, 10 and 11 [15, 20, 22]. This method allows to trace bifurcation manifolds (diagrams) for any type of system model; however, the technique is particularly suited to detect saddle-node bifurcations, yielding a close approximation of the bifurcation point (singularity point) and the corresponding right eigenvector $\mathbf{v}$ [26], without having to actually calculate and trace the system eigenvalues and eigenvectors as the parameter λ changes. The problem with this approach is that it cannot detect Hopf bifurcations, nor differentiate between transcritical and pitchfork bifurcations. For the latter, one needs to check for the transversality conditions of the system at the bifurcation point, which is a costly task. The former needs of the computation of the system equilibria eigenvalues to detect the crossing of the imaginary axis, since the Jacobian J in (10) does not become singular in this case; a very expensive procedure when dealing with relatively large systems. Furthermore, to discern which type of Hopf has taken place (subcritical or supercritical), one needs to run a costly transient simulation or use special techniques that take into considerations additional nonlinear terms in the system [8, 19, 20]. Nevertheless, for PQ load models and typically small resistive losses in the transmission system, Hopf bifurcations are unlikely to occur [10].

Figures 9 and 10 depict the projections of the bifurcation diagram onto different (P, V) planes (P-V nose curves) for various system models. Due to system size, detecting possible occurrences of Hopf bifurcations before a saddle-node was not pursued, since Hopf bifurcations are beyond the scope of this paper. For this reason the author has chosen not to differentiate between s.e.p.s and u.e.p.s in these final figures; nevertheless, one typically expects to have stable equilibria above the saddle-node bifurcation for these system models. In all these figures, the voltage profiles in buses 15 (a 138KV bus located in Machala, a city in the south-west of Ecuador) and 34 (a 138KV bus located in Manabi, a province in the central west coast of Ecuador), were plotted to depict two distinct system nose curves. Bus 34 was particularly chosen since the right and left eigenvectors at the bifurcation point, pinpoint that particular area as the one with the largest reactive power deficits, fully matching the operational knowledge of the actual system. Although the bifurcation diagram projections in Fig. 9(a) do not yield much information regarding the size of the stability region by themselves, the area on the diagrams can be associated to an energy measure due to the PQ load model used in this case, giving an idea of how stable the system is at a particular load level. Furthermore, the parameter λ in this case can be associated to a total MVA system load (1292MVA), yielding a maximum loadability margin of

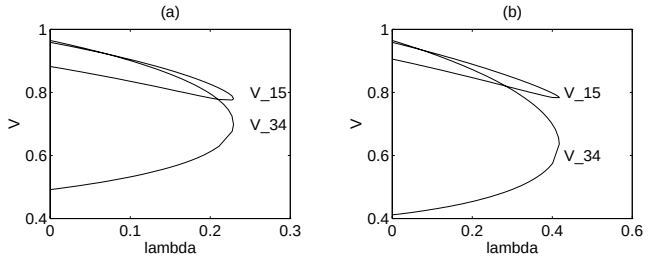

Fig. 9. Bifurcation diagrams of the SNI Ecuadorian system for (a) PQ and (b) mixed load models.

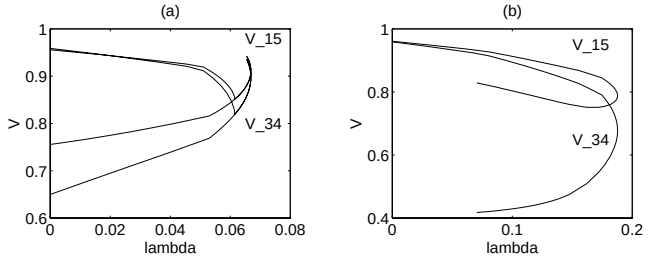

Fig. 10. Bifurcation diagrams of the SNI Ecuadorian system for (a) PQ and (b) mixed load models when Q limits are considered in the generators.

296MVA ($\lambda_{max} = 0.229133$).

In Fig. 9(b), the mixed load model (11) was used to obtain new bifurcations diagrams and a different saddle-node bifurcation. Notice again the wide changes in voltage magnitude at bus 34 for changing loading conditions, indicating once more the lack of reactive power support that is the characteristic of this system. The value of $\lambda_{max} = 0.417712$ is practically twice as mush as the one in the previous case, since now the loads reduced their power demand as the voltages decrease, allowing the system to handle "heavier" loading conditions. The latter comment should be regarded with caution, since the loading level indicated by λ does not have a one-to-one correspondence to MVA loading levels as in the previous figure. Due to the relatively large resistive terms in this system model, one cannot use the simple analogy of the bifurcation diagram area to convey an idea of the size of the stability region for each value of λ; for this particular load model only time simulations can yield the robustness of the system to large perturbations at a given load level. Nevertheless, close to the saddle-node bifurcation one expects the system to have a small stability region due to the merging of the s.e.p and a u.e.p.

Figures. 10 depict the effect of generator Q limits in saddle-node bifurcations. These Q limits were roughly modeled by fixing the reactive power output of the generator at its limits [12], which is not an accurate model, but the approach allows for a first understanding of the general effects of AVR limits in saddle-node bifurcations for different load models. In Figs. 10 one can clearly observe that the Q limits significantly reduce the loadability margin in both cases, since major generating facilities reach maximum reactive power limits, i.e., vapor turbines in El Salitral (located near the largest load center in Ecuador, the coastal city of Guayaquil) at $\lambda = 0.05109 = 66MVA$ in Fig. 10(a), and the Agoyan hydro station (a relatively large generation station in the central Andean region) at $\lambda = 0.1747$ in Fig. 10(b). Furthermore, Fig. 10(a) depicts an immediate system instability at $\lambda = 0.0615 = 79.5MVA$, due to some generators reaching maximum reactive limits at the largest Ecuadorian generating station (Paute, a 1000 MVA hydro complex located in the south central Ecuadorian Andes) and completely losing voltage control of the system. Notice the rather small loadability margin of the system in Fig. 10(a). These particular problems have been detected during the actual system operation,

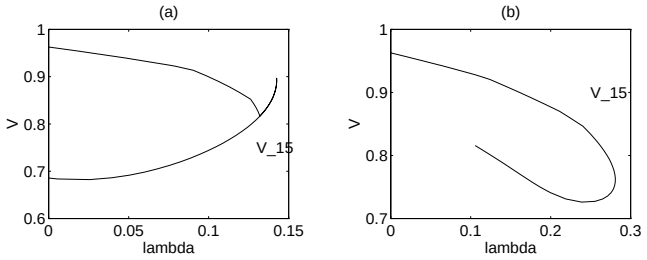

Fig. 11. Bifurcation diagrams of the SNI Ecuadorian system when a 70 MVAR synchronous compensator is placed on bus 34. Figure (a) corresponds to PQ load models, and figure (b) to mixed load models. Q limits are enforced in the generators.

and they are the reason for the repetitive voltage problems throughout the network.

Based on the results of the bifurcation analyses of the previous cases, a 70MVAR synchronous compensator is placed on bus 34, which is one of the possible solutions under consideration at the Ecuadorian utility (INECEL in Spanish) to improve the stability of the SNI system. The new system yields Figs. 11; observe the significant improvement in system loadability. However, Fig. 11(a) still presents a Q limit instability at $\lambda = 0.132 = 170.5MVA$, due to a maximum reactive limit in the hydro generating station of Agoyan.

IV. CONCLUSIONS

The paper has thoroughly discussed the limitations and typical uses of saddle-node bifurcations. The relation between these particular bifurcations and voltage collapse has also been analyzed for several system models. Particularly, the effect of different load models in saddle-node bifurcations has been addressed in a variety of test systems, including a real 115 bus system.

The results from bifurcation studies presented in the paper cannot be dismissed based solely on the idea that the load and system model are not "realistic." Observe that similar arguments can be used to ignore the output of Power Flow studies; research and experience, however, have demonstrated the validity and limitations of these types of analyses. This paper answers the latter two questions pertaining saddle-node bifurcation studies, and demonstrates that these analyses and the related methods are thoroughly valid, as the results for a real system show when compared to the actual operational knowledge of it. Nevertheless, as with any other system analysis technique, the user must discern the usefulness of these results based on the methods and models used.

References

[1] L. H. Fink, ed., *Proceedings: Bulk Power System Voltage Phenomena—Voltage Stability and Security*, EPRI EL-6183, January 1989.

[2] L. H. Fink, ed., *Proceedings: Bulk Power System Voltage Phenomena—Voltage Stability and Security*, ECC/NSF Workshop, Fairfax, VA, Ecc. Inc., August 1991.

[3] *Modelling of Voltage Collapse Including Dynamic Phenomena*, CIGRE Report, Task Force 38-02-10, Draft 3, June 1992.

[4] M. M. Begovic and A. G. Phadke, "Dynamic Simulation of Voltage Collapse," *IEEE Trans. Power Systems*, Vol. 5, No. 1, February 1990, pp. 198–203.

[5] H. G. Kwatny, A. K. Pasrija, L. Y. Bahar, "Static Bifurcations in Electric Power Networks: Loss of Steady-State Stability and Voltage Collapse," *IEEE Trans. Circuits and Syst.*, Vol. 33, No. 10, October 1986, pp. 981–991.

[6] I. Dobson and H. D. Chiang, "Towards a Theory of Voltage Collapse in Electric Power Systems," *Systems & Control Letters*, Vol. 13, 1989, pp. 253–262.

[7] C. A. Cañizares, F. L. Alvarado, C. L. DeMarco, I. Dobson, W. F. Long, "Point of Collapse Methods Applied to AC/DC Power Systems," *IEEE Trans. Power Systems*, Vol. 7, No. 2, May 1992, pp. 673–683.

[8] V. Ajjarapu and B. Lee, "Bifurcation Theory and its Application to Nonlinear Dynamical Phenomena in an Electrical Power System," *IEEE Trans. Power Systems*, Vol. 7, No. 2, February 1992, pp. 424–431.

[9] B. Gao, G. K. Morrison, P. Kundur, "Voltage Stability Evaluation Using Modal Analysis," *IEEE Trans. Power Systems*, Vol. 7, No. 4, November 1992, pp. 1529–1542.

[10] E. H. Abed and P. P. Varaiya, "Nonlinear Oscillations in Power Systems," *International Journal of Electric Power & Energy Systems*, Vol. 6, 1984, pp. 37–43.

[11] P. W. Sauer, B. C. Lesieutre, M. A. Pai, "Dynamic vs. Static Aspects of Voltage Problems," in [2], pp. 207–216.

[12] C. C. Liu and K. T. Vu, "Types of Voltage Collapse," in [2], pp. 133–141.

[13] I. Dobson and L. Lu, "Voltage Collapse Precipitated by the Immediate Change in Stability When Generator Reactive Power Limits are Encountered," *IEEE Trans. Circuits and Syst.–I*, Vol. 39, No. 9, September 1992, pp. 762–766.

[14] G. K. Morrison, B. Gao, P. Kundur, "Voltage Stability Analysis Using Static and Dynamic Approaches," *IEEE Trans. Power Systems*, Vol. 8, No. 3, August 1993, pp. 1159–1171.

[15] C. A. Cañizares and F. L. Alvarado, "Point of Collapse and Continuation Methods for Large AC/DC Systems," *IEEE Trans. Power Systems*, Vol. 8, No. 1, February 1993, pp. 1–8.

[16] M. K. Pal, Discussions to [7, 9, 14, 15, 18].

[17] "National Interconnected System Load Flow: Peak Demand," INECEL, December 1991, in Spanish.

[18] J. Deuse and M. Stubbe, "Dynamic Simulation of Voltage Collapses," *IEEE Trans. Power Systems*, Vol. 8, No. 3, August 1993, pp. 894–904.

[19] J. Guckenheimer and P. Holmes, *Nonlinear Oscillations, Dynamical Systems, and Bifurcations of Vector Fields*, Springer-Verlag, New York, 1986.

[20] R. Seydel, *From Equilibrium to Chaos—Practical Bifurcation and Stability Analysis*, Elsevier Science Publishers, North-Holland, 1988.

[21] P. A. Löf, T. Smed, G. Anderson, D.J. Hill, "Fast Calculation of a Voltage Stability Index," *IEEE Trans. Power Systems*, Vol. 7, No. 1, February 1992, pp. 54–64.

[22] C. A. Cañizares, W. F. Long, F. L. Alvarado, C. L. DeMarco, "Techniques for Detecting Proximity to Voltage Collapse in AC/DC Systems," *Proc. III SEPOPE*, Belo Horizonte, Brazil, May 1992, paper IP-18.

[23] T. J. Overbye anf C. L. DeMarco, "Voltage Security Enhancement Using Energy Based Sensitivities," *IEEE Trans. Power Systems*, Vol. 6, No. 3, August 1991, pp. 1196–1202.

[24] T. J. Overbye, I. Dobson, C. L. DeMarco, "Q-V Curve Interpretations of Energy Measures for Voltage Security," IEEE/PES Winter Meeting, Columbus, OH, January 1993, paper WM 184-2-PWRS.

[25] C. L. DeMarco and C. A. Cañizares, "A Vector Energy Function Approach for Security Analysis of AC/DC Systems," *IEEE Trans. Power Systems*, Vol. 7, No. 3, August 1992, pp. 1001–1011.

[26] C. A. Cañizares, "Saddle-Node Bifurcations in Power Systems," *Proc. JIEE*, Quito, Ecuador, July 1993, pp. 222–229.

[27] I. Dobson, "Observations on the Geometry of Saddle Node Bifurcations and Voltage Collapse in Electrical Power Systems," *IEEE Trans. Circuits and Syst.–I*, Vol. 39, No. 3, March 1992, pp. 240–243.

[28] I. Dobson, "Computing and Optimum Direction in Control Space to Avoid Saddle Node Bifurcation and Voltage Collpase in Electric Power Systems," *IEEE Trans. Automatic Control*, Vol. 37, No. 10, October 1992, pp. 1616–1620.

[29] K. Walve, "Modelling of Power System Components at Severe Disturbances," *Proc. Int. Conf. Large High Voltage Electric Syst.–CIGRE*, August 1986, paper 38-18.

[30] K. Jimma, A. Tomac, K. Vu, C.-C. Liu, "A Study of Dynamic Load Models for Voltage Collapse Analysis," in [2].

[31] S. S. Sastry, "The Effects of Small Noise on Implicitly Defined Nonlinear Dynamical Systems," *IEEE Trans. Circuits and Syst.*, Vol. 30, No. 9, September 1983, pp. 651–663.

[32] C. L. DeMarco and A. R. Bergen, "Application of Singular Perturbation Techniques to Power System Transient Stability Analysis," *Proc. ISCAS*, May 1984, pp. 597–601.

[33] V. Venkatasubramanian, H. Schättler, J. Zaborszky, "A Taxonomy of the Dynamics of the Large Power Systems with Emphasis on Its Voltage Stability," in [2], pp. 9–52.

[34] C. L. DeMarco, "A New Method of Constructing Lyapunov Functions for Power Systems," *Proc. ISCAS*, 1988, pp. 905–908.

[35] M. A. Pai, *Energy Function Analysis for Power System Stability*, Kluwer Academic Publishers, 1989.

[36] M. K. Pal, "Voltage Stability Conditions Considering Load Characteristics," *IEEE Transactions Power Systems*, Vol. 7, No. 1, February 1992, pp. 243–249.

[37] *Load Modeling for Power Flow and Transient Stability Computer Studies*, Vol. 2, EPRI Report EL-5003, January 1987.

Claudio A. Cañizares (S'87, M'91) was born in Mexico, D.F. in 1960. In April 1984, he received the Electrical Engineer diploma from the Escuela Politécnica Nacional (EPN), Quito-Ecuador, where he was a Professor for 9 years, and the MS (1988) and PhD (1991) degrees in Electrical Engineering from the University of Wisconsin–Madison. Dr. Cañizares is currently an Assistant Professor at the University of Waterloo, at the Electrical and Computer Engineering Department, and his research activities are mostly concentrated in the analysis of stability issues in ac/dc systems.